


Erythrocytic Iron Deficiency Enhances Susceptibility to *Plasmodium chabaudi* Infection in Mice Carrying a Missense Mutation in Transferrin Receptor 1

Patrick M. Lelliott, Brendan J. McMorran, Simon J. Foote,  Gaetan Burgio

Australian National University, John Curtin School of Medical Research, Canberra, ACT, Australia, and Macquarie University, Australian School of Advanced Medicine, Sydney, NSW, Australia

The treatment of iron deficiency in areas of high malaria transmission is complicated by evidence which suggests that iron deficiency anemia protects against malaria, while iron supplementation increases malaria risk. Iron deficiency anemia results in an array of pathologies, including reduced systemic iron bioavailability and abnormal erythrocyte physiology; however, the mechanisms by which these pathologies influence malaria infection are not well defined. In the present study, the response to malaria infection was examined in a mutant mouse line, *Tfrc*^{MRI24910}, identified during an *N*-ethyl-*N*-nitrosourea (ENU) screen. This line carries a missense mutation in the gene for transferrin receptor 1 (TFR1). Heterozygous mice exhibited reduced erythrocyte volume and density, a phenotype consistent with dietary iron deficiency anemia. However, unlike the case in dietary deficiency, the erythrocyte half-life, mean corpuscular hemoglobin concentration, and intraerythrocytic ferritin content were unchanged. Systemic iron bioavailability was also unchanged, indicating that this mutation results in erythrocytic iron deficiency without significantly altering overall iron homeostasis. When infected with the rodent malaria parasite *Plasmodium chabaudi adami*, mice displayed increased parasitemia and succumbed to infection more quickly than their wild-type littermates. Transfusion of fluorescently labeled erythrocytes into malaria parasite-infected mice demonstrated an erythrocyte-autonomous enhanced survival of parasites within mutant erythrocytes. Together, these results indicate that TFR1 deficiency alters erythrocyte physiology in a way that is similar to dietary iron deficiency anemia, albeit to a lesser degree, and that this promotes intraerythrocytic parasite survival and an increased susceptibility to malaria in mice. These findings may have implications for the management of iron deficiency in the context of malaria.

Iron deficiency and supplementation can influence the risk and outcome of malaria infection. Epidemiology studies have indicated that iron deficiency anemia (IDA) is associated with a reduced risk of malaria in children and pregnant women (1–5), whereas clinical trials have demonstrated that iron supplementation in the absence of adequate health care increases the risk of malaria (6, 7). While the mechanisms underlying these outcomes are not well defined, it is clear that two major factors contribute: iron bioavailability and erythrocyte physiology.

Iron bioavailability and homeostasis in the host during malaria infection are complex and incompletely understood (8). During infection, expression of the iron-regulatory hormone hepcidin increases significantly, leading to reduced dietary iron absorption and increased iron storage (9–12). The restriction of iron bioavailability may be a host defense mechanism designed to inhibit parasite access to iron, although the source of iron utilized by the parasite is still unclear (13, 14). In liver-stage infection, reduced iron bioavailability brought on by previously established blood-stage infection inhibits the development of sporozoites, thereby preventing compound infections (15). It has been speculated that an excess of iron bioavailability resulting from iron supplementation may subvert these processes and encourage parasite growth (16, 17). Expression of the iron-regulatory protein lipocalin 2 (LCN2) is increased during malaria infection (18), and studies of knockout mice indicate a key role for LCN2 in modulating the innate and adaptive immune responses to infection through its influence on iron recycling (19). It is speculated that LCN2 redistributes iron to control erythropoiesis and immune cell develop-

ment during infection, although it remains to be seen if this may be influenced by iron deficiency or supplementation.

While iron bioavailability can have a direct impact on the outcome of malaria infection, it also affects erythrocyte physiology, the target cell of blood-stage malaria infection. Iron forms part of the heme molecule, which, in complex with hemoglobin, comprises 96% of the dry weight of erythrocytes (20). Iron deficiency impedes normal erythrocyte development, leading to reduced cell volume (microcytosis) and density. Interestingly, *Plasmodium falciparum* invasion and replication are inhibited in iron-deficient erythrocytes compared to normal erythrocytes *in vitro*, although the reason for this has not been determined (21). In rodent malaria, parasitized iron-deficient erythrocytes are more likely to display phosphatidylserine, which results in enhanced phagocytosis of these cells relative to that of equivalent parasitized control

Received 16 July 2015 Returned for modification 9 August 2015

Accepted 20 August 2015

Accepted manuscript posted online 24 August 2015

Citation Lelliott PM, McMorran BJ, Foote SJ, Burgio G. 2015. Erythrocytic iron deficiency enhances susceptibility to *Plasmodium chabaudi* infection in mice carrying a missense mutation in transferrin receptor 1. *Infect Immun* 83:4322–4334. doi:10.1128/IAI.00926-15.

Editor: J. H. Adams

Address correspondence to Gaetan Burgio, Gaetan.Burgio@anu.edu.au.

Supplemental material for this article may be found at <http://dx.doi.org/10.1128/IAI.00926-15>.

Copyright © 2015, American Society for Microbiology. All Rights Reserved.

erythrocytes (22, 23). The reasons for this increased exposure are also undetermined. Overall, evidence suggests that alterations in both iron bioavailability and erythrocyte physiology significantly affect the course of malaria infection, although the biological mechanisms underpinning this remain unclear.

Transferrin receptor 1 (TFR1) is a major protein involved in transporting iron into cells via the iron carrier transferrin and is essential for erythropoiesis (24). It also regulates iron homeostasis through its interaction with the hemochromatosis protein (HFE), which in turn influences hepcidin expression (25–27). Iron-loaded transferrin competes with HFE in binding to TFR1, such that increased or decreased binding sites on TFR1 lead to decreased or increased levels of HFE, respectively, in circulation (28–30). Mice with mutations induced in TFR1 to promote or prevent binding of HFE display decreased or increased hepcidin expression, respectively (26). The expression of TFR1 also affects erythrocyte physiology, with TFR1 deficiency resulting in reduced iron uptake by erythrocyte progenitors and microcytosis in a manner similar to that with dietary iron deficiency (24).

This study investigated the role of TFR1 in iron homeostasis and erythrocyte physiology in the context of rodent malaria infection through the characterization of an *N*-ethyl-*N*-nitrosourea (ENU)-mutagenized mouse line. It was postulated that physiological changes in the erythrocyte, brought on by insufficient iron availability during erythropoiesis due to the lack of TFR1, would impair parasite invasion and replication within these cells. Furthermore, changes in iron homeostasis in these mice were predicted to alter the course of infection by influencing iron bioavailability and modulating the erythropoietic response.

MATERIALS AND METHODS

Mice and ethics. Mice were housed at 21°C with a 12-h–12-h light-dark cycle. Procedures were performed under ethics agreements A0104070, ARA 2012/019, and A2014/054, approved by the animal ethics committees at the University of Tasmania, Macquarie University, and the Australian National University, respectively, and conformed to the National Health and Medical Research Council (NHMRC) Australian code of practice.

ENU mutagenesis screen. Two intraperitoneal injections of ENU at 150 mg/kg of body weight (Sigma-Aldrich, St. Louis, MO) were given 1 week apart to male SJL/J mice. Mice were intercrossed with female SJL/J mice, and progeny (G1) were bled at 7 weeks of age and screened for their peripheral blood parameters, using an Advia 120 automated hematological analyzer (Siemens, Berlin, Germany). The MRI24910 mouse was selected because it exhibited a mean cell volume (MCV) more than 3 standard deviations below the mean. Heritability was ascertained by progeny (G2) testing.

Linkage analysis and sequencing. Linkage analysis was used to determine the genomic interval containing the mutation responsible for the microcytic (MCV of <48 fl) phenotype. Microcytic G2 mice were outcrossed with C57BL/6 mice to produce F1 offspring. Microcytic F1 mice were crossed with C57BL/6 mice to produce N2 offspring. DNAs were extracted from 13 microcytic N2 mice by using DNeasy blood and tissue kits (Qiagen, Limburg, Netherlands). A genome-wide single nucleotide polymorphism (SNP) analysis was performed on a MASS array platform with over 300 polymorphic SNPs, using IPlex Gold technology (Sequenom Inc., San Diego, CA). This was performed by the Australian Genome Research Facility (AGRF). The genomic interval was confirmed by PCR amplification of a polymorphic microsatellite marker (D16Mit12) in 43 additional microcytic N2 mice. *Tfrc* exons, including intron-exon borders, were amplified via PCR, and Sanger sequencing was performed by the AGRF.

Osmotic fragility measurement. Ten-microliter aliquots of blood from mutant and wild-type mice were incubated for 30 min at room temperature in 1 ml of 20 mM phosphate buffer (pH 7.4) containing between 0 and 10 g/liter NaCl. The absorbance of the supernatant at 540 nm was used to determine hemolysis.

Erythrocyte half-life assay. Mice were injected intravenously (i.v.) with 1 mg sulfosuccinimidyl-6-(biotinamido)hexanoate (Thermo Fisher Scientific, Waltham, MA) in mouse tonicity phosphate-buffered saline (MT-PBS), resulting in approximately 99% biotinylation of erythrocytes. Tail blood samples were taken on the indicated days and prepared for flow cytometry as described below. The percentage of remaining biotinylated cells on each day was recorded.

Erythrocyte density assay. Erythrocyte density was determined based on separation of erythrocytes in a discontinuous Percoll gradient. A 90% (vol/vol) Percoll solution in MTRC (154 mM NaCl, 5.6 mM KCl, 1 mM MgCl₂, 2.2 mM CaCl₂, 20 mM HEPES, 10 mM glucose, 30 U/ml heparin, 0.5% bovine serum albumin [BSA], pH 7.4; 0.22- μ m filter sterilized) was prepared and then diluted in MTRC to produce eight solutions of decreasing density. These solutions were carefully layered in a 15-ml Falcon tube, from the most dense to the least dense. Freshly obtained blood was layered on top of the gradient before centrifugation at 800 \times g for 30 min at 4°C. Each layer was collected, erythrocytes were lysed in hypotonic solution, and the absorbance of the supernatant at 540 nm was measured. The proportion of erythrocytes in each density layer was calculated as the sample absorbance divided by the total absorbance for all layers for that blood sample.

Staining of splenic erythrocyte progenitors for flow cytometry. For the characterization of erythropoietic cells, whole spleens were dissociated through a 70- μ m cell strainer, and approximately 1×10^7 cells were incubated in 50 μ l of 1- μ g/ml anti-CD16/CD32 (eBioscience, San Diego, CA) in MTRC for 15 min at 37°C to prevent nonspecific antibody binding. Cells were then incubated for 30 min at 37°C in the dark with 1 μ g/ml anti-TER119–phycoerythrin (PE)–Cy7, 1 μ g/ml anti-CD71 (TFR1)–peridinin chlorophyll protein (PerCP)–eFluor 710 (eBioscience, San Diego, CA), and 4 μ M Hoechst 33342 (Sigma-Aldrich, St. Louis, MO) and analyzed by flow cytometry.

Measurement of cell surface TFR1. Because TFR1 molecules undergo a constant endocytosis cycle in the presence of iron, spleen cells were first washed in MTRC to remove excess iron. Cells were then incubated at 37°C for 15 min to allow TFR1 molecules to return to the surface of the cell before proceeding with antibody staining as described above. The amount of cell surface TFR1 was determined by the mean fluorescence intensity (MFI) of staining with the CD71 (TFR1) antibody.

Iron measurements. Total nonheme iron was measured as described by Patel et al. (31). Briefly, tissue samples (~50 to 100 mg) were dried at 45°C for 48 h before being digested in 300 μ l of 10% trichloroacetic acid–10% HCl at 65°C for 48 h. The iron concentration was determined based on the absorbance at 535 nm after incubation with a chromogen solution (0.01% bathophenanthroline-disulfonic acid, 0.1% thioglycolic acid, 2.5 M sodium acetate), with comparison to a standard curve.

Serum and erythrocytic ferritin levels were measured using a mouse ferritin enzyme-linked immunosorbent assay (ELISA) kit (Kamiya Biomedical, Seattle, WA). The labile iron pool (LIP) was measured as described by Prus and Fibach (32). Briefly, spleen cells were incubated with 2 μ M calcein-aceto-methyl ester (CA-AM) (Sigma-Aldrich, St. Louis, MO) for 15 min at 37°C. Cells were washed and divided between two tubes. Deferiprone (100 μ M) (L1; Sigma-Aldrich, St. Louis, MO) was added to one tube, and the cells were incubated for 1 h at 37°C before being analyzed by flow cytometry. The LIP was calculated by subtracting the CA-AM MFI of L1-treated cells from that of untreated cells. For spleen histology, tissue was fixed in 4% formalin for 24 h and then embedded in paraffin wax. Sections were stained using Perls's Prussian Blue solution of 5% potassium ferrocyanide and 5% HCl at a 1:1 ratio (33).

RNA extraction and quantitative PCR. RNAs were extracted from livers by use of TRIzol (Life Technologies, Carlsbad, CA). Reverse tran-

scription was performed using anchored oligo(dT)₁₈ primers and a Transcriptor High Fidelity cDNA synthesis kit (Roche, Basel, Switzerland). Quantitative PCR was performed with GoTaq qPCR master mix (Bio-Rad, Hercules, CA), using primers for *Hamp1* (F, 5'-TTGCGATACCAA TGCAGAAGA-3'; and R, 5'-GATGTGGCTCTAGGCTATGTT-3') and *Actb* (F, 5'-GGCTGTATCCCCTCCATCG-3'; and R, 5'-CCAATGGT AACAATGCCATGT-3') which were designed so that one primer spanned an exon-exon boundary. Results were calculated using the $\Delta\Delta C_T$ method and reported as the fold change in cDNA of the mutant compared to the wild type, based on *Hamp1* expression compared to *Actb* expression.

Malaria infection. For experimental malaria infection, 250 μ l of thawed *Plasmodium chabaudi adami* DS- or *Plasmodium yoelii* NL-parasitized blood was injected into the intraperitoneal cavity of C57BL/6 donor mice. Once C57BL/6 donors reached 2 to 15% parasitemia, they were bled by cardiac puncture. Parasitized blood was diluted in Krebs's buffered saline containing 0.2% glucose according to the method of Jarra and Brown (34), and the required dose of parasitized erythrocytes was injected into the intraperitoneal cavity of mice to be infected. For one experiment, parasitized blood was diluted in minimum essential medium with 10% HEPES (Sigma-Aldrich, St. Louis, MO) and injected intravascularly. All experiments were performed on SJL/J mice unless otherwise stated.

Microscopy. Thin blood smears were fixed in methanol for 1 min before being stained in a 10% Giemsa solution (Sigma-Aldrich, St. Louis, MO) at pH 7.4 for 10 min. Parasitemia was calculated by counting at least 500 parasitized cells by light microscopy at a magnification of $\times 100$.

Labeled-erythrocyte assays. Labeled-erythrocyte assays were performed as previously described (35, 36), with modifications. Briefly, blood was collected from wild-type and mutant mice by cardiac puncture and suspended at 20% hematocrit in MTR (154 mM NaCl, 5.6 mM KCl, 1 mM MgCl₂, 2.2 mM CaCl₂, 20 mM HEPES, 10 mM glucose, 30 U/ml heparin, pH 7.4; 0.22- μ m filter sterilized). Blood was incubated with 20 μ g/ml hydroxysulfosuccinimide Atto 633 or 20 μ g/ml hydroxysulfosuccinimide Atto 488 (Sigma-Aldrich, St. Louis, MO) at 4°C for 1 h with constant slow mixing. Erythrocytes were washed three times, and mutant erythrocytes were combined with wild-type erythrocytes in approximately equal proportions in two label combinations to account for any dye effects. Approximately 1×10^9 to 2×10^9 labeled erythrocytes were transfused intravascularly into infected wild-type and mutant mice during schizogony (approximately 6 h into the dark cycle). Blood samples were taken from recipient mice at the indicated time points and stained and analyzed by flow cytometry as described below. The percentage of infected mutant labeled erythrocytes was divided by the percentage of infected wild-type labeled erythrocytes to obtain the ratio of parasitized mutant cells for each individual host mouse. The one-sample *t* test was used to determine the statistical significance of this value at each time point. Similarly, the ratio of remaining labeled cells was calculated as the percentage of remaining mutant labeled cells (compared to the first time point) divided by the percentage of remaining wild-type labeled cells.

Staining of blood samples for flow cytometry. For measurements of erythrocyte half-life, parasitemia, and reticulocytosis, erythrocyte counts, and labeled-erythrocyte assays, samples were prepared for flow cytometry as follows. Three microliters of tail blood was collected directly into 50 μ l staining solution which contained 2 μ l Sphero blank calibration beads (only for assays measuring erythrocyte counts) (BD Biosciences, Franklin Lakes, NJ), 1 μ g/ml streptavidin-PE-Cy7 (only for assays with biotinylated erythrocytes), 1 μ g/ml anti-CD45-allophycocyanin (APC)-eFluor 780 (clone 30-F11), and 1 μ g/ml anti-CD71 (TFR1)-PerCP-eFluor 710 (clone R17217) (eBioscience, San Diego, CA) in MTRC. Samples were incubated at room temperature for 20 min, 500 μ l of 2 μ M Hoechst 34580 (Sigma-Aldrich, St. Louis, MO) was added, and samples were incubated at room temperature for a further 20 min before being washed and analyzed by flow cytometry.

Flow cytometry. Samples were run and 1,000,000 to 10,000,000 events were collected using either BD FACS Diva or BD FACS Software with a

BD Aria II, BD LSRFortessa, or BD Influx flow cytometer (BD Biosciences, Franklin Lakes, NJ). Analysis was performed using FlowJo v10.0.6 (Tree Star, Ashland, OR). Cell debris and noise were removed from analysis based on forward scatter (FSC) and side scatter (SSC) properties, and single cells were gated based on the FSC peak area/height ratio. Beads were selected based on FSC/SSC, and relative erythrocyte counts were determined based on the bead counts for infected mice versus three uninfected mice included in each analysis.

Statistics. For malaria survival, statistical significance was determined by the Mantel-Cox test. Linkage analysis scores were calculated based on a chi-square goodness-of-fit test. For ratios obtained in the labeled-erythrocyte assays, significance was determined using the one-sample *t* test, with 1 as the hypothetical mean. For other results, two-tailed Student's *t* test was used to determine statistical significance.

RESULTS

Identification of a novel ENU-induced mutation in *Tfrc* in a mouse strain with a dominant microcytosis phenotype. Automated full blood counts were performed on 7-week-old G1 offspring from ENU-mutagenized mice to identify dominant mutations causing erythrocyte abnormalities. The G1 mouse MRI24910 was selected based on a decreased mean cell volume (MCV) of 45.9 fl, which was more than 3 standard deviations below the mean (53.1 ± 1.3 fl) (Fig. 1A). Half of the G2 mice, generated by backcrossing the G1 founder to wild-type mice, also displayed this phenotype (mean MCV, 46.8 ± 0.6 fl), indicating that a fully penetrant, dominant mutation was causing the microcytosis (Fig. 1A and C). Apart from their size, the microcytic erythrocytes displayed a normal, discoid shape, with no other obvious abnormalities (Fig. 1B). Additional parameters from the automated full blood counts indicated that affected mice had reduced erythrocyte hemoglobin, which was compensated for by an increased erythrocyte count and resulted in a normal level of hemoglobin by blood volume (Fig. 1C). Microcytic erythrocytes had significantly decreased osmotic fragility, as assessed by the extent of hemolysis of erythrocytes in different concentrations of salt solution (Fig. 1D). To investigate the *in vivo* half-life of erythrocytes, mice were injected with biotin, and the proportion of biotinylated erythrocytes was monitored over time. No difference was found in the clearance rate of microcytic erythrocytes (Fig. 1E). Percoll density gradient centrifugation indicated that microcytic cells had a reduced density (Fig. 1F).

The ENU-induced mutation responsible for this phenotype was mapped by backcrossing the original G1 mouse, MRI24910, to a C57BL/6 mouse. Linkage analysis using affected mice (MCV of <48 fl) indicated a significant linkage peak on chromosome 16, between 7 Mbp and 67 Mbp (see Fig. S1A and B in the supplemental material). The *Tfrc* gene, located at 32.6 Mbp, was selected as an ideal candidate. A deficiency in this gene has been reported to cause a similar dominant microcytosis phenotype (24). Sanger sequencing of all exons of the *Tfrc* gene revealed a T-to-C transition in exon 5 leading to a serine-to-proline substitution (S161P) (see Fig. S1C). No other mutations in the gene were identified. Serine 161 is highly conserved across different species (Fig. 2B) and is located in a so-called protease-like domain of the transferrin receptor 1 protein (TFR1), which in the equivalent region of the human protein is involved in the binding of transferrin (37) (Fig. 2A). It was hypothesized that the mutation, designated *Tfrc*^{MRI24910}, may disrupt normal TFR1 function in a way that causes perturbations in erythropoietic iron transport, thereby explaining the abnormal erythrocyte phenotype of these mice.

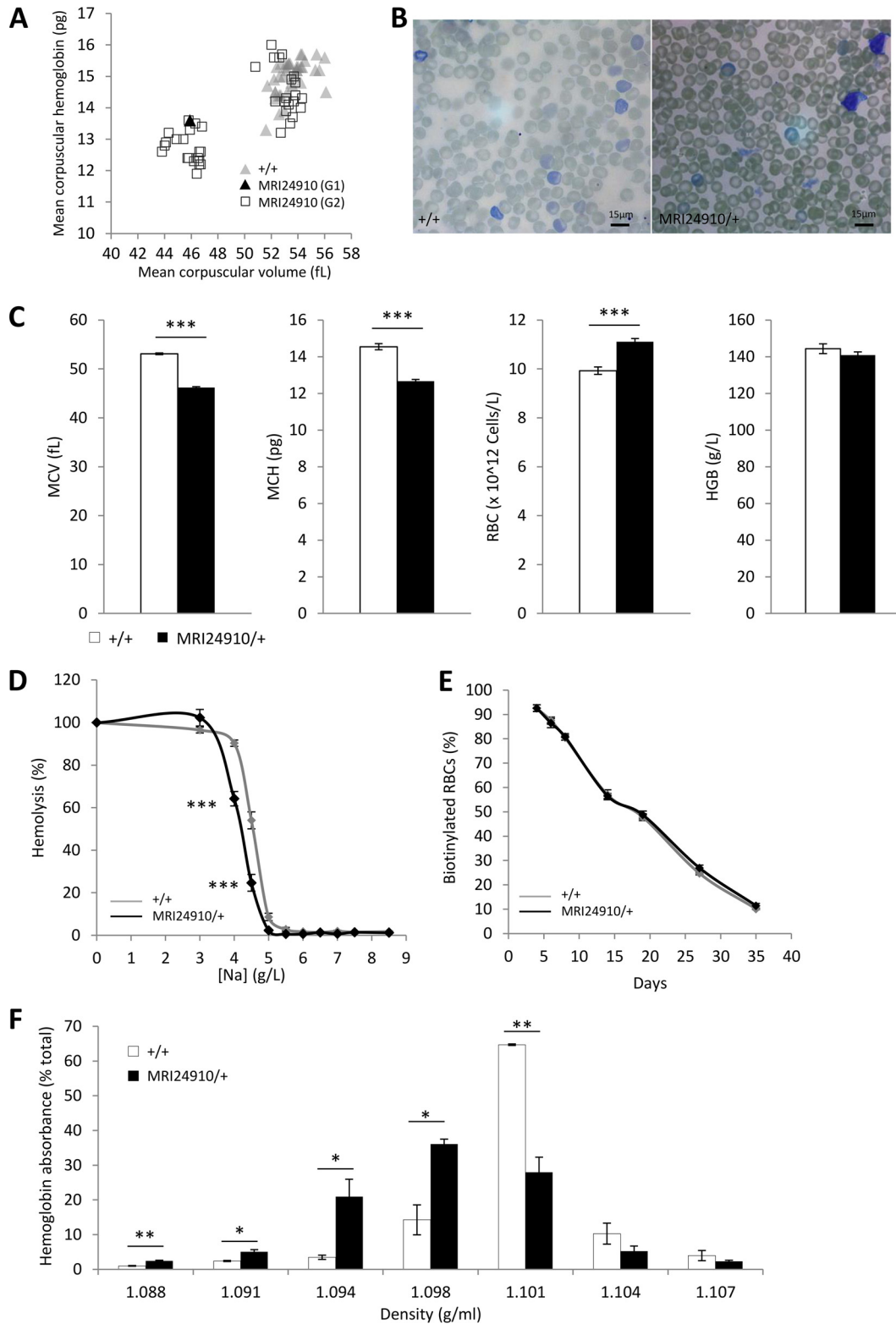
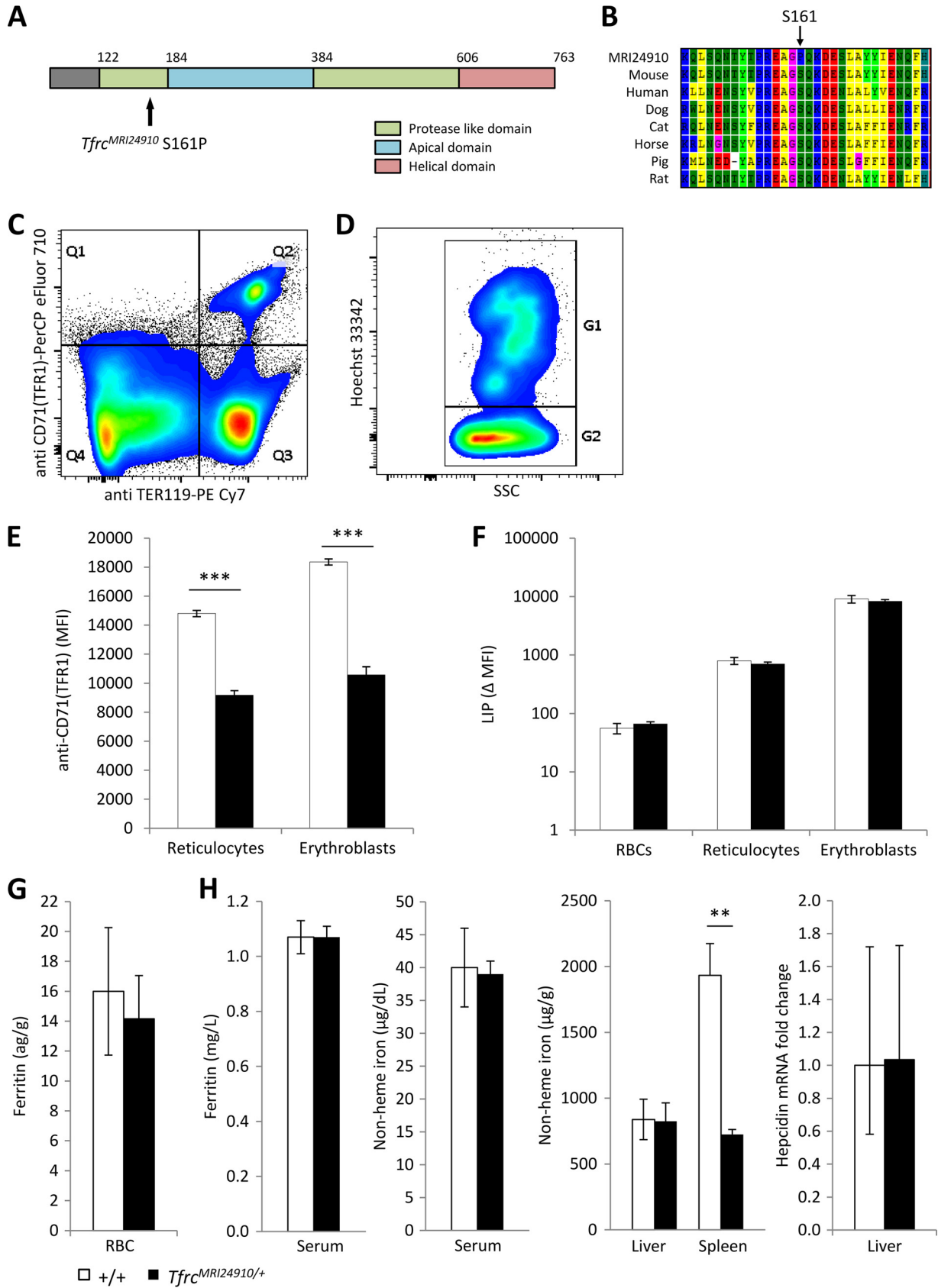


FIG 1 Hematological properties of the MRI24910 mutant line. (A) Blood parameters measured in ENU-mutagenized offspring, including the G1 mouse MRI24910, and G2 offspring. G2 mice exist in two populations, at a Mendelian ratio of 1:1. Mice were assumed to be carrying the mutation if their MCV was <48 fl and are referred to as MRI24910/+ or mutant mice, while mice with MCVs of >48 fl are referred to as wild type (+/+). (B) Giemsa-stained blood smears of wild-type and mutant mice. (C) Hematological parameters from automated blood counts. MCV, mean corpuscular volume; MCH, mean corpuscular hemoglobin; RBC, erythrocyte count; HGB, total hemoglobin by blood volume. (D) Osmotic fragility of erythrocytes based on hemolysis in salt solutions. (E) Erythrocyte half-lives, based on the percentage of biotinylated cells remaining in circulation after an initial biotin injection that labeled >99% of erythrocytes. (F) Quantification of the relative number of erythrocytes, based on hemoglobin absorbance, in each density layer of a discontinuous Percoll gradient. Error bars indicate standard errors of the means (SEM). *, $P < 0.05$; **, $P < 0.01$; ***, $P < 0.001$. Data are from four experiments with a total of 20 mice per group for the automated blood counts. Data are from one experiment with 7 to 9 mice per group for the osmotic fragility test and with 4 mice per group for the erythrocyte half-life and density measurements.



Repeated attempts to generate homozygous *Tfrc*^{MRI24910} animals were unsuccessful, and there was evidence of embryo reabsorption in heterozygous females mated with heterozygous males at embryonic day 13.5, indicating that two mutant alleles prevent viable embryo development. Throughout this study, *Tfrc*^{MRI24910/+} mice are referred to as mutants.

***Tfrc*^{MRI24910} results in reduced TFR1 expression and altered splenic iron homeostasis.** To investigate the effect of the *Tfrc*^{MRI24910} mutation on TFR1 expression, the cell surface levels of TFR1 were measured on splenic erythroblasts and reticulocytes, which express particularly high levels of TFR1 (38). TFR1 transports iron into the cell through endocytosis, and only a proportion of the protein is present on the cell surface at any one time. Cells were therefore incubated in iron-free medium to stimulate and maximize the externalization of the protein before analysis. Cells were then stained with anti-CD71 (TFR1) antibody, and also Hoechst DNA dye and anti-TER119, to facilitate the identification of erythroblasts and reticulocytes by flow cytometry (Fig. 2C and D). The TER119 antigen is specifically expressed on late-stage murine erythroid cells, while the DNA-specific Hoechst dye can be used to distinguish between enucleate reticulocytes and late-stage erythroblasts. The mean fluorescence intensity (MFI) of staining with the CD71 (TFR1) antibody was used to quantify levels of surface TFR1. Splenic erythroblasts and reticulocytes from mutant mice had significantly less surface TFR1 per cell than did those from wild-type mice, based on mean fluorescence intensity (38% and 42% less, respectively) (Fig. 2E). The reduced expression may have been caused by either haploinsufficiency or the mutant protein not undergoing normal trafficking to the surface of the cell. In either case, a reduction in surface-expressed TFR1 would likely reduce the cell's ability to import iron, and therefore would perturb erythropoietic development.

To investigate if the decreased surface expression of TFR1 alters cellular iron management during erythropoiesis, the labile iron pool (LIP) of erythrocytes, reticulocytes, and erythroblasts, as well as intraerythrocytic ferritin content, was measured. Cellular iron homeostasis and TFR1 expression within erythroblasts are tightly regulated by the iron-regulatory proteins Irp1 and Irp2, which in turn sense the cellular LIP status (39–41). An excess LIP results in upregulation of ferritin expression, while a small LIP leads to increased expression of TFR1. Analysis of the LIP in erythroid progenitors (erythroblasts and reticulocytes) as well as erythrocytes found no difference between mutant and wild-type cells (Fig. 2F). In addition, intraerythrocytic ferritin levels were also found to be normal in mutant mice (Fig. 2G). There was also no difference in the proportion of splenic erythroblasts and reticulocytes between mutants and wild-type mice and no difference in the proportion of peripheral blood reticulocytes (see Fig. S2A and B in the supplemental material). Overall, these results indicate

that the *Tfrc*^{MRI24910} mutation causes reduced surface expression of TFR1 but does not result in any major perturbations to cellular iron homeostasis. Erythroblasts are able to mature into apparently normal functioning erythrocytes, albeit of a reduced size and reduced hemoglobin content.

The iron-regulatory protein HFE binds to TFR1. Therefore, a reduction in TFR1 could plausibly lead to an increase in the amount of circulating HFE, disturbing hepcidin levels and affecting systemic iron homeostasis (26). Levels of ferritin and non-heme-bound iron in the sera and livers of the mutant mice appeared normal. In contrast, non-heme-bound iron in the spleen was significantly reduced (Fig. 2H). This was confirmed by histological analysis of spleen sections by use of Perls's Prussian Blue (see Fig. S3 in the supplemental material). The spleen is directly involved in erythropoiesis and erythrocyte iron recycling. Since cellular iron homeostasis and the abundance of splenic erythropoietic cells were normal (Fig. 2F and G; see Fig. S2), this result could instead indicate an abnormality in the recycling of erythrocytes. An abnormality in erythrocyte recycling could be caused by an impairment of macrophage phagocytosis or a change in the susceptibility of erythrocytes to splenic clearance. Together, these results suggest that systemic iron availability is essentially normal in mutant mice.

***Tfrc*^{MRI24910} increases susceptibility to *P. chabaudi adami* DS infection but not to *P. yoelii* NL infection.** We next investigated if the *Tfrc*^{MRI24910} mutation would influence the course of malaria infection. Mice were challenged with the rodent malaria parasites *P. chabaudi adami* DS and *P. yoelii* NL, and parasitemia and survival were monitored daily. During *P. chabaudi* infection, parasitemias of mutant mice increased more rapidly than those of their wild-type littermates, resulting in significantly higher parasitemias during the acute stage of infection, before peak parasitemia (Fig. 3A). After the peak of infection, parasitemias decreased at equal rates in both mutant and wild-type mice. SJL/J mice are naturally susceptible to *P. chabaudi* infection and rarely survive when challenged with this strain. Nevertheless, mutant mice succumbed to infection earlier than wild-type mice, although the difference in survival was not significant ($P = 0.067$) (Fig. 3B). In contrast, both mutant and wild-type mice responded similarly to the less virulent *P. yoelii* infection. Parasitemias of mice increased at equivalent rates, and mice were able to clear infection equally well, with no mice succumbing to infection (Fig. 4A). Notably, *P. yoelii* infects reticulocytes at a higher frequency than that for mature erythrocytes, while *P. chabaudi* infects mainly mature erythrocytes, suggesting that the enhanced susceptibility of mutant mice may be restricted to differences in the interaction of parasites with mature erythrocytes. To investigate this hypothesis, we measured the parasitemia of the mature erythrocyte population during *P. yoelii* infection. There was a modest increase in

FIG 2 Identification and characterization of the MRI24910 mutation in *Tfrc*. (A) An S161P point mutation was located in the protease-like domain of TFR1. (B) The S161 residue is highly conserved, suggesting that it has a critical function in the protein. (C) Splenic erythroblasts and reticulocytes were identified based on positive staining with the markers TER119 and CD71 (TFR1) (Q2), and erythrocytes were identified based on negative CD71 and positive TER119 staining (Q3). (D) From the Q2 gate, erythroblasts (G1) were distinguished from reticulocytes (G2) based on Hoechst staining. (E) The MFI of staining with anti-CD71 (TFR1) was determined for each cell population as a measure of TFR1 surface expression. (F) Labile iron pool (LIP) of each cell population, determined based on the change in CA-AM MFI, with or without the iron chelator L1, according to the method of Prus and Fibach (32). (G) Ferritin contents in erythrocytes (G) and serum (H) were measured by ELISA. (H) Nonheme iron contents in the serum, liver, and spleen were measured colorimetrically, and hepcidin mRNA expression in the liver relative to that of the wild type was determined using the beta-actin gene as a housekeeping gene. Error bars indicate SEM. **, $P < 0.01$; ***, $P < 0.001$. Data are representative of one of three experiments with four mice per group for TFR1 MFI. Data are from one experiment with four mice per group for LIP, ferritin, serum iron, and hepcidin measurements and from two experiments with seven or eight mice per group for liver and spleen iron measurements.

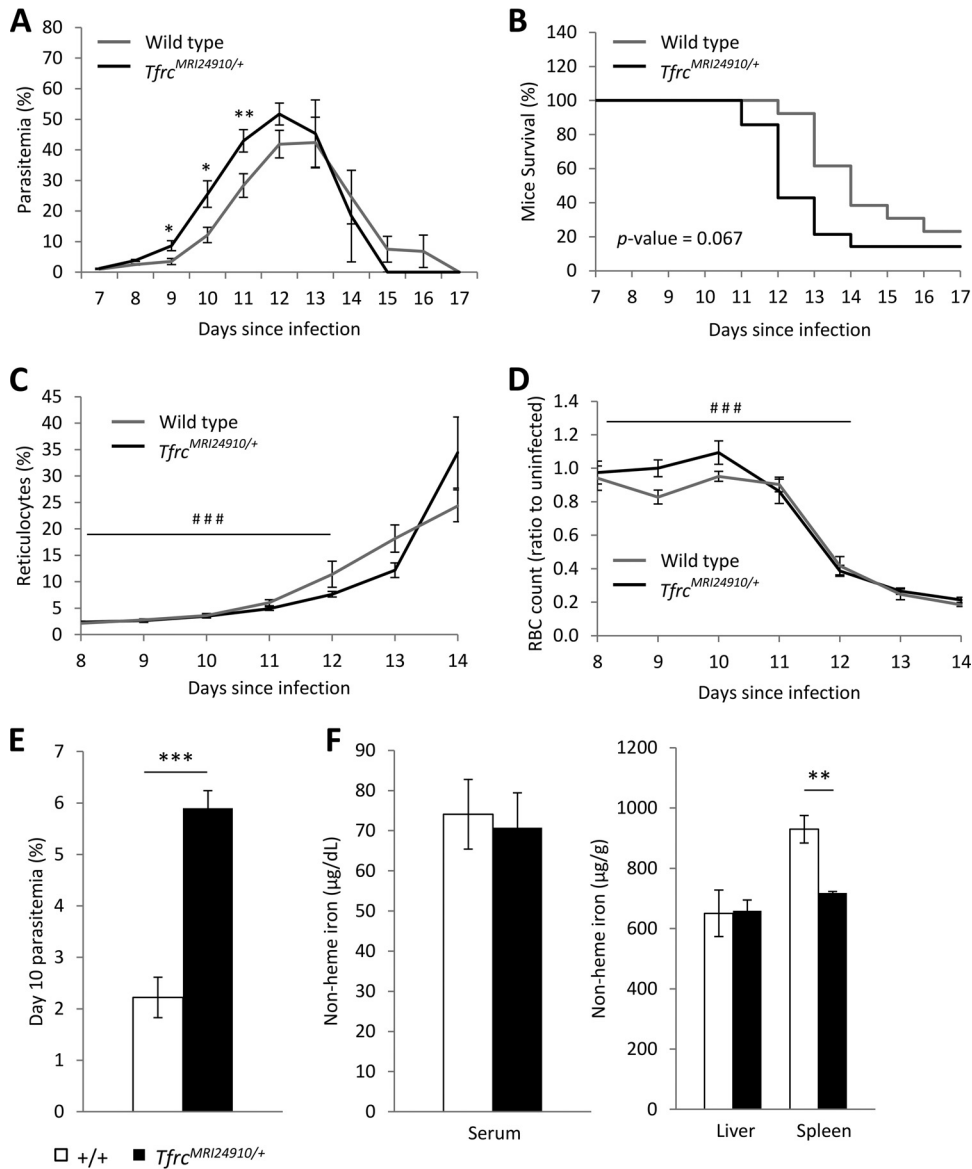


FIG 3 Susceptibility of *Tfrc*^{MRI24910/+} mice to *P. chabaudi adami* DS infection. Female mice were infected with 1×10^4 parasitized erythrocytes by intraperitoneal injection and analyzed for parasitemia (A) and survival (B). Data are combined from three experiments with a total of 14 mutant and 13 wild-type mice. Parasitemia was determined by either counting of cells on Giemsa-stained slides (experiments 1 and 2) or flow cytometry using the DNA dye Hoechst 34580 (experiment 3). Reticulocyte (C) and erythrocyte (D) counts were determined by flow cytometry in one experiment (six mutant and four wild-type mice). Parasitemia (E) and nonheme iron levels in the serum, liver, and spleen (F) were determined in one experiment with mice infected with 1×10^4 parasitized erythrocytes by intravenous injection and sacrificed on day 10 of infection (four mutant and five wild-type mice). Error bars indicate SEM; the log rank (Mantel-Cox) test was used to calculate *P* values for survival. *, *P* < 0.05; **, *P* < 0.01; ***, *P* < 0.001 (between wild-type and mutant mice). ###, *P* < 0.001 between day 12 and day 8 of infection.

P. yoelii parasitemia of mature erythrocytes, although this was statistically significant only on day 5 (Fig. 4B).

We considered two possible reasons for the increased susceptibility of the mutant erythrocytes to *P. chabaudi* infection. First, the mutation may impose a systemic effect on the erythropoietic response or iron homeostasis. Alternatively, physiological changes to the erythrocyte itself may enhance the ability of the parasite to invade or to grow or survive within the mutant erythrocyte.

To address the first hypothesis, the erythropoietic response and iron homeostasis were investigated during the course of *P. cha-*

baudi infection. To assess the erythropoietic response, erythrocyte counts and the proportion of reticulocytes were measured. Reticulocyte abundance increased significantly, in concordance with decreasing erythrocyte numbers (Fig. 3C and D). However, there were no differences between mutant and wild-type mice. We also quantified the splenic erythroblasts and reticulocytes in a cohort of mice on day 10 of infection, but no differences were observed between mutant and wild-type mice (see Fig. S2B in the supplemental material). In addition, analysis of the erythropoietic response in mutant versus normal mice during *P. yoelii* infection showed that the responses were no different (Fig. 4D and E). To-

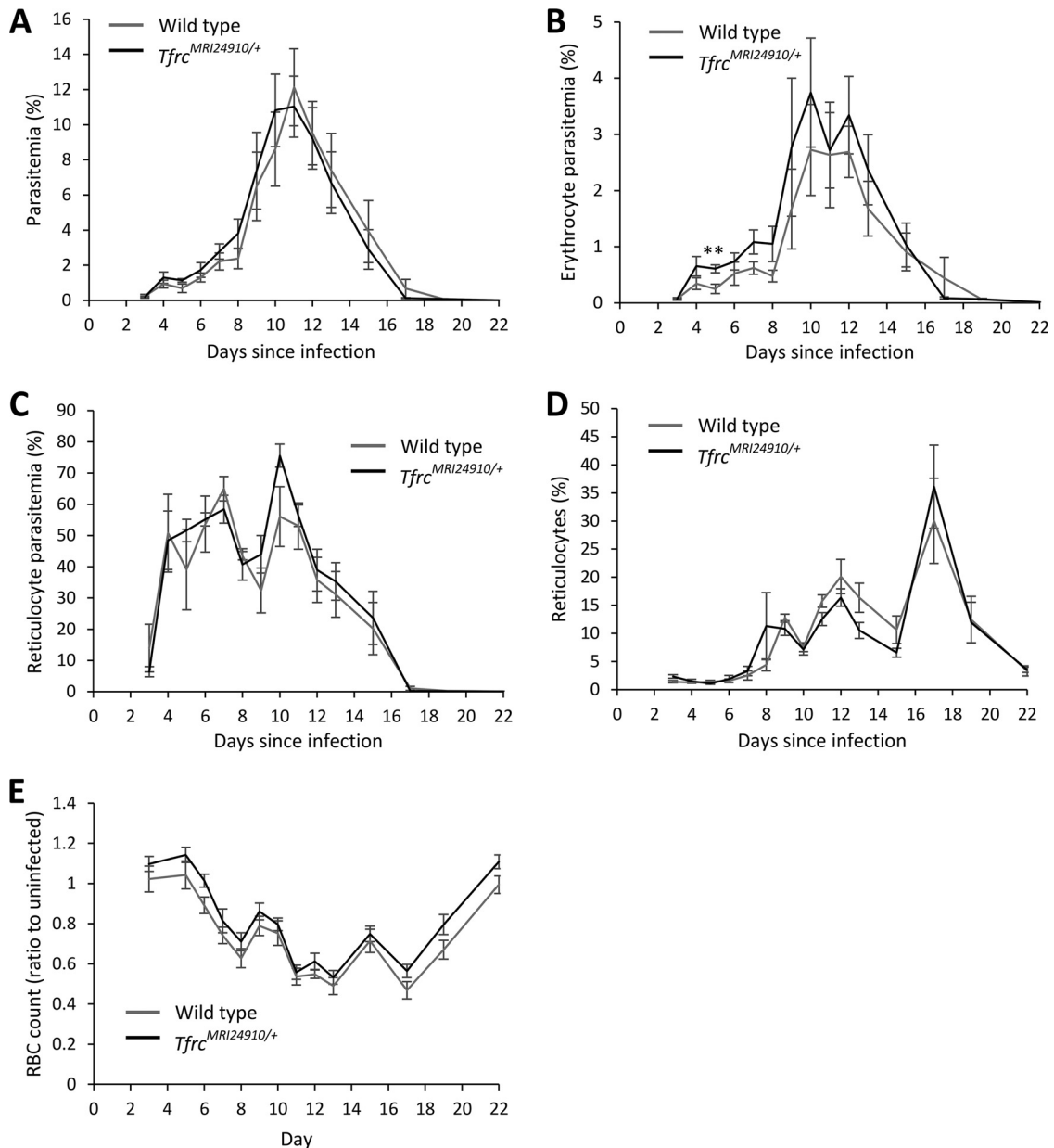
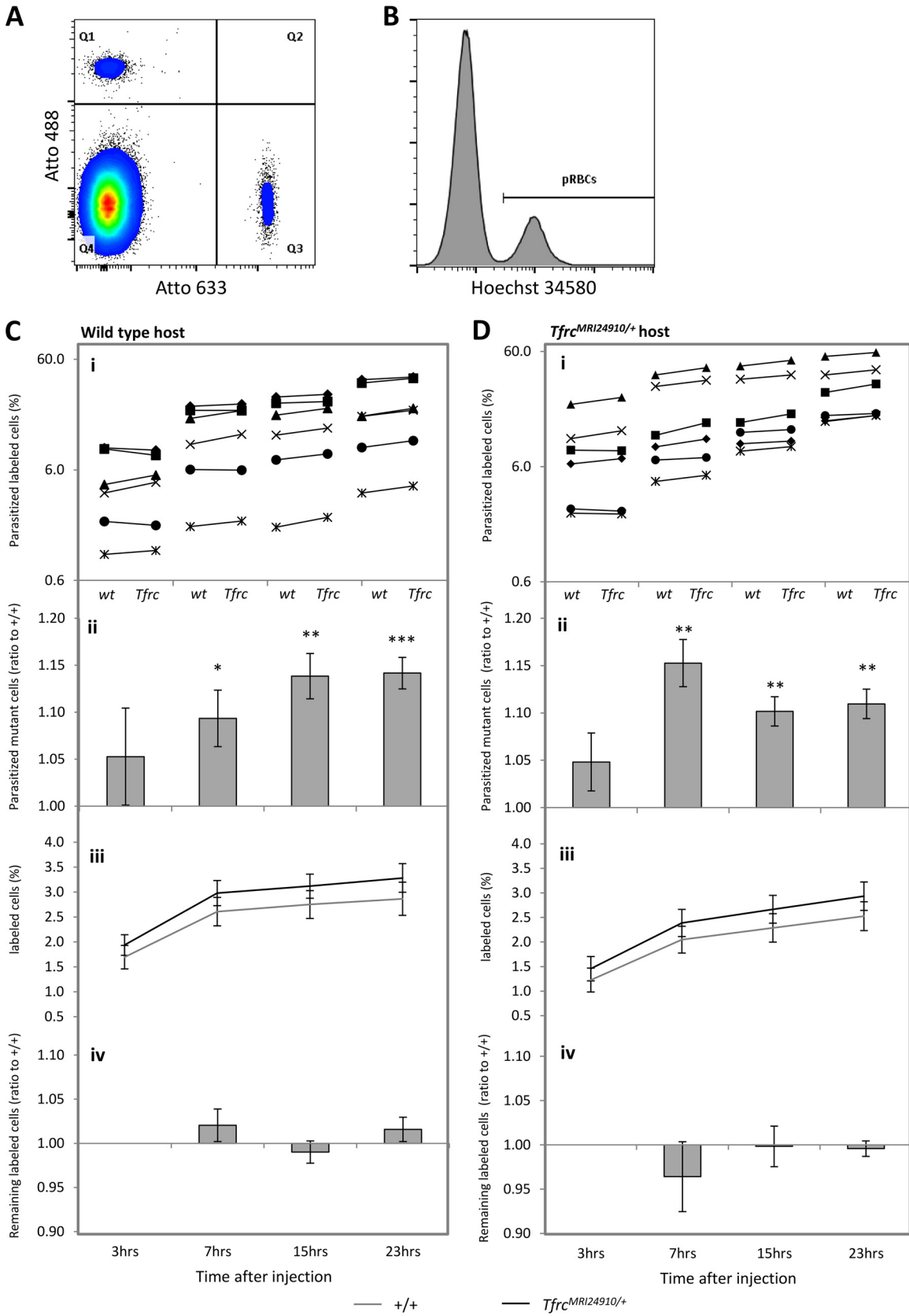


FIG 4 *P. yoelii* NL infection of *Tfrc^{MRI24910/+}* mice. Overall parasitemias (A), mature erythrocyte parasitemias (B), reticulocyte parasitemias (C), reticulocyte counts (D), and erythrocyte counts (E) were determined by flow cytometry. Mice were infected with 1×10^5 parasitized erythrocytes. Error bars indicate SEM. **, $P < 0.01$ between wild-type and mutant mice. All data are from one experiment with 5 to 7 female mice per group.

gether, these results indicate that the erythropoietic response to malaria infection is not affected by the *Tfrc^{MRI24910}* mutation.

During malaria infection, the parasite must obtain iron from its host in order to survive and replicate. The host may sequester iron during infection in order to restrict parasite growth (42). Serum and tissue iron levels were measured in a cohort of mice on day 10 of infection. Although mutant mice had significantly higher parasitemias, there were no differences in serum or liver iron levels to indicate abnormal iron homeostasis during infection (Fig. 3E and F), while spleen iron levels remained reduced in mutant mice, as observed when mice were uninfected (Fig. 3F). Together, these results suggest that the increased parasitemias of mutant mice were not related to iron homeostasis.

To investigate if intrinsic differences in the mutant erythrocyte instead determined the infection susceptibility phenotype, we investigated the ability of parasites to invade mutant erythrocytes and the survival of parasitized cells within the circulation. We employed a labeled-erythrocyte assay as previously described (35, 36). The assay allows a direct comparison of parasite invasion and survival in two different erythrocyte populations within the circulation of a single host animal (Fig. 5A and B). For *P. chabaudi* infection, time points spanning one complete replication cycle were investigated (3, 7, 15, and 23 h) (Fig. 5C). After injection of labeled mutant and wild-type cells into an infected wild-type host animal, the number and relative proportion of labeled cells remained relatively stable over the course of the experiment, indi-



cating that uninfected mutant cells were normally tolerated in the host animal (Fig. 5C, panels iii and iv). After 3 h, there were no significant differences in the proportions of parasitized labeled cells in the host animals (Fig. 5C, panels i and ii). This indicates that the parasite was able to invade each cell type with an equal efficiency. However, at the last three time points, robust and statistically significant increases in the ratios were observed, namely, 1.09 ± 0.032 ($P = 0.026$), 1.14 ± 0.024 ($P = 0.002$), and 1.14 ± 0.017 ($P = 0.0003$), respectively (Fig. 5C, panel ii). This represents a 9 to 14% relative increase in the number of mutant parasitized cells. Similar differences at these three time points, in terms of both magnitude and statistical significance, were observed in equivalent experiments using infected mutant mice as the host animals (Fig. 5D, panel ii). Taken together, the results suggest that *P. chabaudi* parasites have an erythrocyte-autonomous survival advantage when residing within mutant erythrocytes, which occurs regardless of the host environment and across a range of host parasitemias.

The same assay was also performed using *P. yoelii*-infected host animals, except that an extended series of time points were examined (12, 36, and 60 h) (Fig. 6). For technical reasons, we focused only on proportions of mature erythrocytes and could not examine early, invasion-dependent time points because of the small number of erythrocytes infected. The proportions of labeled mature cells remained stable over the course of the experiment, although there was a modest decrease compared to all circulating cells (Fig. 6A, panels iii and iv). Similar to the results obtained using *P. chabaudi*, significantly larger proportions of *P. yoelii*-parasitized mutant cells were observed at each time point: 1.64 ± 0.10 ($P = 0.0002$), 1.13 ± 0.052 ($P = 0.04$), and 1.13 ± 0.016 ($P = 0.00003$), respectively (Fig. 6A, panels i and ii). This indicates that the enhanced survival of parasitized mutant erythrocytes appears to occur irrespective of parasite species. The ratio differences in the *P. yoelii* experiments were also seen in both wild-type and mutant host animals, confirming the cell-autonomous nature of this phenotype (Fig. 6B).

Overall, these results suggest that although parasites invade mutant and wild-type erythrocytes equally, they have an erythrocyte-autonomous survival advantage in mutant erythrocytes. Although this survival increase was modest (9 to 15%), the cumulative effect of this survival advantage over multiple parasite replication cycles could plausibly explain the increased parasitemias of mutant mice during *P. chabaudi* infection.

DISCUSSION

Iron homeostasis during malaria infection is complex and remains poorly understood (8). Clinical studies have shown 30 to 51% reductions in the risk of malaria in children with iron defi-

ciency anemia (IDA) compared to children with normal iron levels (1–3). Evidence suggests that altered iron bioavailability and erythrocyte physiology may explain this reduced malaria risk; however, the relative importance of these factors and the mechanisms involved remain unclear. In the present study, the response to malaria was assessed in a mouse line carrying a novel ENU-induced missense mutation in the *Tfrc* gene. Given the critical role of TFR1 in facilitating iron uptake by erythroblasts, as well as its influence on systemic iron homeostasis, it was hypothesized that this mutation would reduce malaria susceptibility in a manner similar to that for IDA. In fact, the opposite was found to be true, with mutant mice displaying an increased susceptibility to *P. chabaudi* infection.

There are several key differences between IDA and the mouse line described here. IDA occurs due to dietary iron deficiency, where a systemic lack of iron leads to an inadequate iron supply during erythropoiesis, resulting in microcytosis and a reduced mean cell hemoglobin level, blood count, overall hemoglobin level, mean cell hemoglobin concentration, and hematocrit. IDA erythrocytes also display reduced osmotic fragility, density, ferritin content, and erythrocyte half-life (43). Mutant mice exhibited a less severe erythrocytic iron deficiency, as indicated by microcytosis and a reduced mean cell hemoglobin level, osmotic fragility, and density but a normal mean cell hemoglobin concentration, ferritin level, and erythrocyte half-life. Additionally, microcytosis was accompanied by an increased blood count, resulting in a normal overall hemoglobin level and hematocrit. Previously characterized mutant mouse lines displaying microcytosis and reduced surface levels of TFR1 on erythroblasts, including the heterozygous knockout mouse line *Tfrc*^{-/+}, exhibit a similar phenotype (24, 44, 45). Given that we also observed reduced TFR1 on the surfaces of mutant erythroblasts, our explanation for the microcytosis in the *Tfrc*^{MRI24910/+} line is a reduction of iron transport into cells during erythropoiesis. It appears that the mice are able to compensate by producing larger numbers of cells. Additionally, the mutation does not result in major perturbations to systemic iron homeostasis, as indicated by normal serum iron parameters, hepcidin expression, and liver iron content.

In addition to investigating the effect of the *Tfrc*^{MRI24910} mutation on iron homeostasis and erythrocyte physiology, the other major focus of this study was determining if this mutation would alter malaria susceptibility. The mechanisms underlying malaria resistance in IDA are still unclear, and this study provided an opportunity to assess the importance of iron deficiency in the erythropoietic system, compared to dietary iron deficiency, in determining malaria risk. Unexpectedly, mutant mice displayed a marked increase in parasitemia during the acute stage of infection with *P. chabaudi*, with a concomitant decrease in survival. We

FIG 5 Enhanced survival of *P. chabaudi* parasites within *Tfrc*^{MRI24910/+} erythrocytes. (A) Transfused erythrocytes from mutant and wild-type mice were identified according to their fluorescent label, either Atto 488 (Q1) or Atto 633 (Q3). (B) For each labeled population, parasitemia was determined according to Hoechst 34580 fluorescence. pRBCs, parasitized red blood cells. (C and D) Analysis of labeled cells transfused into wild-type (wt) (C) or mutant (D) host animals infected with *P. chabaudi*. Six wild-type and six mutant host animals received donor erythrocyte mixtures, labeled as follows: wild type-Atto 488/mutant-Atto 633 or wild type-Atto 633/mutant-Atto 488. Mutant and wild-type donor erythrocytes were obtained from three mutant mice or three wild-type mice and pooled before labeling. Analysis was conducted at the four time points indicated. (i) The percentage of parasitized labeled cells was calculated for each donor erythrocyte population (wt and *Tfrc*) in each host animal (represented by different symbols). (ii) The parasitized mutant cell ratio represents the mean (and SEM) mutant/wild-type ratio calculated from the data shown in panels i. (iii) Percentages of labeled cells represent the proportions of labeled cells (mutant or wild type) relative to host erythrocytes. (iv) Ratios of remaining labeled cells represent the proportions of labeled cells at 7, 15, and 23 h relative to those of labeled cells at 3 h. Error bars indicate SEM. *, $P < 0.05$; **, $P < 0.01$; ***, $P < 0.001$ (as determined using the one-sample *t* test, with a ratio of 1 as the hypothetical mean for each time point).

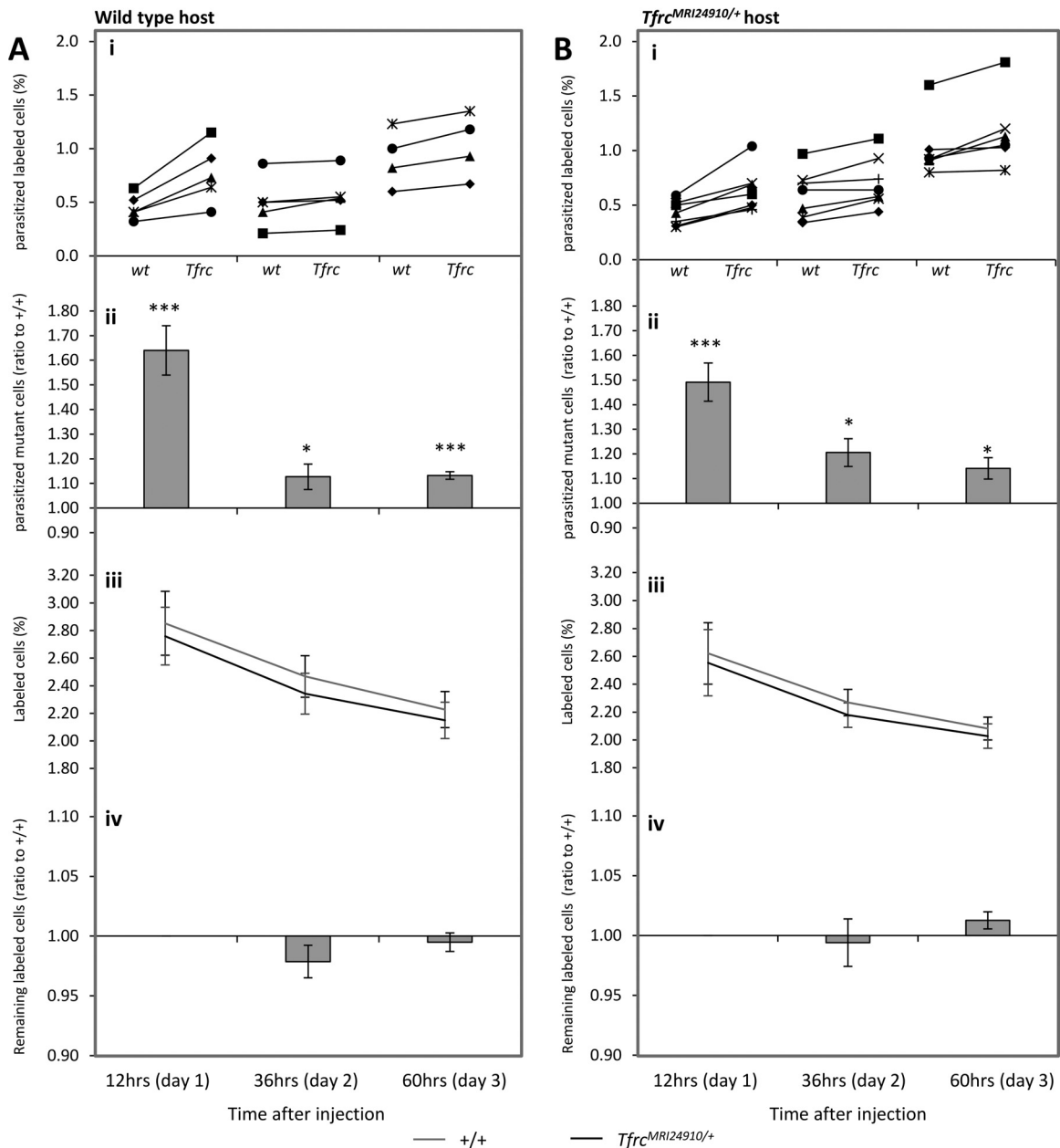


FIG 6 Enhanced survival of *P. yoelii* parasites within *Tfrc^{MRI24910/+}* erythrocytes. Analysis was performed on labeled cells transfused into wild-type (A) or mutant (B) host animals infected with *P. yoelii*. Five wild-type and seven mutant host animals each received donor erythrocyte mixtures, labeled as follows: wild type-Atto 488/mutant-Atto 633 or wild type-Atto 633/mutant-Atto 488. Mutant and wild-type donor erythrocytes were obtained from three mice each and pooled before labeling. Analysis was conducted at the three time points indicated, and data in panels i to iv are presented as described in the legend to Fig. 5. Error bars indicate SEM. *, $P < 0.05$; **, $P < 0.01$; ***, $P < 0.001$ (as determined using the one-sample t test, with a ratio of 1 as the hypothetical mean for each time point).

therefore sought to identify the mechanistic basis of this increased susceptibility.

Malaria infection results in a redistribution of host iron in order to limit iron availability to the invading parasite (15, 19). It has been suggested that parasite growth is inhibited during IDA due to an additional reduction in the bioavailability of iron (46). While it remains unclear where and how the parasite obtains the iron necessary for growth, evidence suggests that the parasite meets some of its need by importing iron from serum (16, 47, 48). Reduced serum iron in individuals with IDA may reduce the parasite's ac-

cess to iron, thereby inhibiting growth. However, systemic iron availability in the *Tfrc^{MRI24910/+}* line was normal, and when the mice were challenged with *P. chabaudi*, no obvious changes in iron homeostasis were observed. We also considered if the mutation impaired the response of mice to the anemia that occurs during malaria infection. Reticulocyte levels and erythrocyte counts were comparable between mutant and wild-type mice during the course of both *P. chabaudi* and *P. yoelii* infections, while spleen erythroblast and reticulocyte levels were also equivalent at the acute stage of *P. chabaudi* infection. Overall, our results indicated

that the systemic response to malaria, in terms of iron homeostasis and erythropoiesis, was normal in mutant mice and could not explain the increased malaria susceptibility.

Erythrocytes from patients with IDA inhibit parasite invasion and growth *in vitro* (21, 23). Therefore, we considered whether altered erythrocyte physiology could account for the observed increase in malaria susceptibility in mutant mice. We did not observe any difference in the ability of *P. chabaudi* parasites to invade mutant erythrocytes in an *in vivo* parasite invasion assay. However, we found that both *P. chabaudi* and *P. yoelii* parasites had an increased survival rate after infecting mutant erythrocytes. The parasite survival phenotypes were equivalent in both wild-type and mutant host animals. This allowed us to conclude that the survival effect is intrinsic to the mutant erythrocyte and is unlikely to be influenced by other host factors affected by the mutation. Erythrocyte-specific factors that influence parasite survival in the circulation include the intracellular environment in which the parasite can grow, maintenance of cell integrity, interaction with immune surveillance and cell clearance mechanisms, and passage through the small capillaries and filtering beds in the spleen. The effects imparted by the *Tfrc*^{MRI24910} mutation on parasitized erythrocytes could potentially affect one or more of these processes. This finding is at odds with the case for IDA erythrocytes, in which the parasite is more susceptible to clearance and therefore has a reduced rate of survival (22, 23). Enhanced clearance in individuals with IDA is thought to be caused by increased phosphatidylserine exposure, which mediates increased phagocytosis, although the reasons for this increased exposure are unknown (22). Our results indicate that physiological characteristics, including microcytosis, density, and osmotic fragility of erythrocytes, do not necessarily influence erythrocyte susceptibility to invasion or the ability of erythrocytes to support parasite growth. This finding is also supported by other studies, both *in vivo* and *in vitro*, which indicate that microcytosis *per se* does not inhibit parasite growth or reduce the risk of malaria (49, 50). These findings may have implications for the management of malaria risk during dietary iron deficiency and suggest that it may be worthwhile to consider malaria risk in cases of low-level iron deficiency, which may result in a phenotype similar to that observed here, as well as severe iron deficiency.

It is highly likely that the erythrocyte-intrinsic increase in parasite survival within the circulation is the principle reason for the observed increase in susceptibility to *P. chabaudi* infection. We did observe a reduction in nonheme splenic iron levels in both infected and uninfected mutant animals, which is indicative of a defect in the erythrocyte recycling system. This could potentially affect the functions of this organ during malarial infection, including cell filtration and macrophage phagocytosis. However, proportions of *P. yoelii*-infected reticulocytes were similar in both mutant and wild-type mice, suggesting that the clearance of these cells was not perturbed. Any contribution to the *P. chabaudi* susceptibility phenotype by the splenic defect is probably minimal, although a more formal examination of this and other immune response functions is required to completely rule out nonerythrocytic factors.

In conclusion, this study reports a novel mutation in *Tfrc* which reduces the surface expression of the encoded protein on erythroblasts. Phenotypically, the mutation causes an erythrocytic iron deficiency, characterized by microcytosis and reduced cell hemoglobin, in heterozygous mice. Importantly, differences in

erythrocyte half-life, mean cell hemoglobin concentration, and intraerythrocytic ferritin content indicate that the erythrocytic iron deficiency of these mice is less severe than that seen in IDA. Unlike mice with IDA, *Tfrc*^{MRI24910} mutant mice displayed an elevated susceptibility to *P. chabaudi* malaria infection and exhibited increased parasitemias during the acute phase of infection, with increased parasitemia levels resulting from an erythrocyte-autonomous increase in parasite survival.

ACKNOWLEDGMENTS

We acknowledge Shelley Lampkin for assistance in maintaining mouse colonies and for helping us to perform malaria infections and Preethi Mayura-Guru for assistance in hematological analysis of mice. We also thank Ian Cockburn for generously supplying the *P. yoelii* parasite strain and lending out space in the animal facility.

We acknowledge funding support from the National Health and Medical Research Council (grants APP605524, 490037, and 1047082), the Australian Research Council (grant DP12010061), the National Collaborative Research Infrastructure Strategy of Australia, and the education investment fund from the Department of Innovation, Industry, Science and Research. P.M.L. is a recipient of an Australian postgraduate award.

P.M.L. performed the experiments, analyzed the data, helped to conceive the study, and wrote the manuscript. B.J.M., S.J.F., and G.B. conceived the study, interpreted the data, and assisted in writing the manuscript.

REFERENCES

- Nyakeriga AM, Troye-Blomberg M, Dorfman JR, Alexander ND, Back R, Kortok M, Chemtai AK, Marsh K, Williams TN. 2004. Iron deficiency and malaria among children living on the coast of Kenya. *J Infect Dis* 190:439–447. <http://dx.doi.org/10.1086/422331>.
- Gwamaka M, Kurtis JD, Sorensen BE, Holte S, Morrison R, Mutabingwa TK, Fried M, Duffy PE. 2012. Iron deficiency protects against severe Plasmodium falciparum malaria and death in young children. *Clin Infect Dis* 54:1137–1144. <http://dx.doi.org/10.1093/cid/cis010>.
- Jonker FA, Calis JC, van Hensbroek MB, Phiri K, Geskus RB, Brabin BJ, Leenstra T. 2012. Iron status predicts malaria risk in Malawian preschool children. *PLoS One* 7:e42670. <http://dx.doi.org/10.1371/journal.pone.0042670>.
- Kabyemela ER, Fried M, Kurtis JD, Mutabingwa TK, Duffy PE. 2008. Decreased susceptibility to Plasmodium falciparum infection in pregnant women with iron deficiency. *J Infect Dis* 198:163–166. <http://dx.doi.org/10.1086/589512>.
- Sangare L, van Eijk AM, Ter Kuile FO, Walson J, Stergachis A. 2014. The association between malaria and iron status or supplementation in pregnancy: a systematic review and meta-analysis. *PLoS One* 9:e87743. <http://dx.doi.org/10.1371/journal.pone.0087743>.
- Veenemans J, Milligan P, Prentice AM, Schouten LR, Inja N, van der Heijden AC, de Boer LC, Jansen EJ, Koopmans AE, Enthoven WT, Kraaijenhagen RJ, Demir AY, Uges DR, Mbugi EV, Savelkoul HF, Verhoef H. 2011. Effect of supplementation with zinc and other micronutrients on malaria in Tanzanian children: a randomised trial. *PLoS Med* 8:e1001125. <http://dx.doi.org/10.1371/journal.pmed.1001125>.
- Sazawal S, Black RE, Ramsan M, Chwaya HM, Stoltzfus RJ, Dutta A, Dhingra U, Kabole I, Deb S, Othman MK, Kabole FM. 2006. Effects of routine prophylactic supplementation with iron and folic acid on admission to hospital and mortality in preschool children in a high malaria transmission setting: community-based, randomised, placebo-controlled trial. *Lancet* 367: 133–143. [http://dx.doi.org/10.1016/S0140-6736\(06\)67962-2](http://dx.doi.org/10.1016/S0140-6736(06)67962-2).
- Prentice AM. 2008. Iron metabolism, malaria, and other infections: what is all the fuss about? *J Nutr* 138:2537–2541. <http://dx.doi.org/10.3945/jn.108.098806>.
- de Mast Q, Nadjm B, Reyburn H, Kemna EH, Amos B, Laarakkers CM, Silalye S, Verhoef H, Sauerwein RW, Swinkels DW, van der Ven AJ. 2009. Assessment of urinary concentrations of hepcidin provides novel insight into disturbances in iron homeostasis during malarial infection. *J Infect Dis* 199:253–262. <http://dx.doi.org/10.1086/595790>.
- Cercamondi CI, Egli IM, Ahouandjinou E, Dossa R, Zeder C, Salami L, Tjalsma H, Wiegierinck E, Tanno T, Hurrell RF, Hounhouigan J,

- Zimmermann MB. 2010. Afebrile *Plasmodium falciparum* parasitemia decreases absorption of fortification iron but does not affect systemic iron utilization: a double stable-isotope study in young Beninese women. *Am J Clin Nutr* 92:1385–1392. <http://dx.doi.org/10.3945/ajcn.2010.30051>.
11. de Mast Q, Syafruddin D, Keijmel S, Riekerink TO, Deky O, Asih PB, Swinkels DW, van der Ven AJ. 2010. Increased serum hepcidin and alterations in blood iron parameters associated with asymptomatic *P. falciparum* and *P. vivax* malaria. *Haematologica* 95:1068–1074. <http://dx.doi.org/10.3324/haematol.2009.019331>.
 12. Atkinson SH, Armitage AE, Khandwala S, Mwangi TW, Uyoga S, Bejon PA, Williams TN, Prentice AM, Drakesmith H. 2014. Combinatorial effects of malaria season, iron deficiency, and inflammation determine plasma hepcidin concentration in African children. *Blood* 123:3221–3229. <http://dx.doi.org/10.1182/blood-2013-10-533000>.
 13. Scholl PF, Tripathi AK, Sullivan DJ. 2005. Bioavailable iron and heme metabolism in *Plasmodium falciparum*. *Curr Top Microbiol Immunol* 295:293–324.
 14. Clark MA, Goheen MM, Cerami C. 2014. Influence of host iron status on *Plasmodium falciparum* infection. *Front Pharmacol* 5:84. <http://dx.doi.org/10.3389/fphar.2014.00084>.
 15. Portugal S, Carret C, Recker M, Armitage AE, Goncalves LA, Epiphonio S, Sullivan D, Roy C, Newbold CI, Drakesmith H, Mota MM. 2011. Host-mediated regulation of superinfection in malaria. *Nat Med* 17:732–737. <http://dx.doi.org/10.1038/nm.2368>.
 16. Clark M, Fisher NC, Kasthuri R, Cerami Hand C. 2013. Parasite maturation and host serum iron influence the labile iron pool of erythrocyte stage *Plasmodium falciparum*. *Br J Haematol* 161:262–269. <http://dx.doi.org/10.1111/bjh.12234>.
 17. Schumann K, Kroll S, Romero-Abal ME, Georgiou NA, Marx JJ, Weiss G, Solomons NW. 2012. Impact of oral iron challenges on circulating non-transferrin-bound iron in healthy Guatemalan males. *Ann Nutr Metab* 60:98–107. <http://dx.doi.org/10.1159/000336177>.
 18. Coban C, Ishii KJ, Uematsu S, Arisue N, Sato S, Yamamoto M, Kawai T, Takeuchi O, Hisaeda H, Horii T, Akira S. 2007. Pathological role of Toll-like receptor signaling in cerebral malaria. *Int Immunol* 19:67–79.
 19. Zhao H, Konishi A, Fujita Y, Yagi M, Ohata K, Aoshi T, Itagaki S, Sato S, Narita H, Abdelgeli NH, Inoue M, Culleton R, Kaneko O, Nakagawa A, Horii T, Akira S, Ishii KJ, Coban C. 2012. Lipocalin 2 bolsters innate and adaptive immune responses to blood-stage malaria infection by reinforcing host iron metabolism. *Cell Host Microbe* 12:705–716. <http://dx.doi.org/10.1016/j.chom.2012.10.010>.
 20. Weed RI, Reed CF, Berg G. 1963. Is hemoglobin an essential structural component of human erythrocyte membranes? *J Clin Invest* 42:581–588. <http://dx.doi.org/10.1172/JCI104747>.
 21. Clark MA, Goheen MM, Fulford A, Prentice AM, Elnagheeb MA, Patel J, Fisher N, Taylor SM, Kasthuri RS, Cerami C. 2014. Host iron status and iron supplementation mediate susceptibility to erythrocytic stage *Plasmodium falciparum*. *Nat Commun* 5:4446. <http://dx.doi.org/10.1038/ncomms5446>.
 22. Matsuzaki-Moriya C, Tu L, Ishida H, Imai T, Suzue K, Hirai M, Tetsutani K, Hamano S, Shimokawa C, Hisaeda H. 2011. A critical role for phagocytosis in resistance to malaria in iron-deficient mice. *Eur J Immunol* 41:1365–1375. <http://dx.doi.org/10.1002/eji.201040942>.
 23. Koka S, Foller M, Lamprecht G, Boini KM, Lang C, Huber SM, Lang F. 2007. Iron deficiency influences the course of malaria in *Plasmodium berghei* infected mice. *Biochem Biophys Res Commun* 357:608–614. <http://dx.doi.org/10.1016/j.bbrc.2007.03.175>.
 24. Levy JE, Jin O, Fujiwara Y, Kuo F, Andrews NC. 1999. Transferrin receptor is necessary for development of erythrocytes and the nervous system. *Nat Genet* 21:396–399. <http://dx.doi.org/10.1038/7727>.
 25. Gao J, Chen J, Kramer M, Tsukamoto H, Zhang AS, Enns CA. 2009. Interaction of the hereditary hemochromatosis protein HFE with transferrin receptor 2 is required for transferrin-induced hepcidin expression. *Cell Metab* 9:217–227. <http://dx.doi.org/10.1016/j.cmet.2009.01.010>.
 26. Schmidt PJ, Toran PT, Giannetti AM, Bjorkman PJ, Andrews NC. 2008. The transferrin receptor modulates Hfe-dependent regulation of hepcidin expression. *Cell Metab* 7:205–214. <http://dx.doi.org/10.1016/j.cmet.2007.11.016>.
 27. Muckenthaler MU, Rodrigues P, Macedo MG, Minana B, Brennan K, Cardoso EM, Hentze MW, de Sousa M. 2004. Molecular analysis of iron overload in beta2-microglobulin-deficient mice. *Blood Cells Mol Dis* 33:125–131. <http://dx.doi.org/10.1016/j.bcmd.2004.05.003>.
 28. Waheed A, Parkkila S, Saarnio J, Fleming RE, Zhou XY, Tomatsu S, Britton RS, Bacon BR, Sly WS. 1999. Association of HFE protein with transferrin receptor in crypt enterocytes of human duodenum. *Proc Natl Acad Sci U S A* 96:1579–1584. <http://dx.doi.org/10.1073/pnas.96.4.1579>.
 29. Lebron JA, Bjorkman PJ. 1999. The transferrin receptor binding site on HFE, the class I MHC-related protein mutated in hereditary hemochromatosis. *J Mol Biol* 289:1109–1118. <http://dx.doi.org/10.1006/jmbi.1999.2842>.
 30. West AP, Jr, Giannetti AM, Herr AB, Bennett MJ, Nangiana JS, Pierce JR, Weiner LP, Snow PM, Bjorkman PJ. 2001. Mutational analysis of the transferrin receptor reveals overlapping HFE and transferrin binding sites. *J Mol Biol* 313:385–397. <http://dx.doi.org/10.1006/jmbi.2001.5048>.
 31. Patel BN, Dunn RJ, Jeong SY, Zhu Q, Julien JP, David S. 2002. Ceruloplasmin regulates iron levels in the CNS and prevents free radical injury. *J Neurosci* 22:6578–6586.
 32. Prus E, Fibach E. 2008. Flow cytometry measurement of the labile iron pool in human hematopoietic cells. *Cytometry A* 73:22–27.
 33. Perls M. 1867. Nachweis von Eisenoxyd in gewissen Pigmenten. *Eur J Pathol* 39:42–48.
 34. Jarra W, Brown KN. 1985. Protective immunity to malaria: studies with cloned lines of *Plasmodium chabaudi* and *P. berghei* in CBA/Ca mice. I. The effectiveness and inter- and intra-species specificity of immunity induced by infection. *Parasite Immunol* 7:595–606.
 35. Lelliott PM, Lampkin S, McMorrnan BJ, Foote SJ, Burgio G. 2014. A flow cytometric assay to quantify invasion of red blood cells by rodent *Plasmodium* parasites in vivo. *Malar J* 13:100. <http://dx.doi.org/10.1186/1475-2875-13-100>.
 36. Lelliott PM, McMorrnan BJ, Foote SJ, Burgio G. 2015. In vivo assessment of rodent *Plasmodium* parasitemia and merozoite invasion by flow cytometry. *J Vis Exp* 2015:e52736. <http://dx.doi.org/10.3791/52736>.
 37. Giannetti AM, Snow PM, Zak O, Bjorkman PJ. 2003. Mechanism for multiple ligand recognition by the human transferrin receptor. *PLoS Biol* 1:E51.
 38. Iacopetta BJ, Morgan EH. 1983. Transferrin endocytosis and iron uptake during erythroid cell development. *Biomed Biochim Acta* 42:S182–S186.
 39. Konijn AM, Glickstein H, Vaisman B, Meyron-Holtz EG, Slotki IN, Cabantchik ZI. 1999. The cellular labile iron pool and intracellular ferritin in K562 cells. *Blood* 94:2128–2134.
 40. Klausner RD, Rouault TA, Harford JB. 1993. Regulating the fate of mRNA: the control of cellular iron metabolism. *Cell* 72:19–28. [http://dx.doi.org/10.1016/0092-8674\(93\)90046-S](http://dx.doi.org/10.1016/0092-8674(93)90046-S).
 41. Leibold EA, Guo B. 1992. Iron-dependent regulation of ferritin and transferrin receptor expression by the iron-responsive element binding protein. *Annu Rev Nutr* 12:345–368. <http://dx.doi.org/10.1146/annurev.nu.12.070192.002021>.
 42. Weinberg ED. 1978. Iron and infection. *Microbiol Rev* 42:45–66.
 43. Yip R, Mohandas N, Clark MR, Jain S, Shohet SB, Dallman PR. 1983. Red cell membrane stiffness in iron deficiency. *Blood* 62:99–106.
 44. Galy B, Ferring D, Minana B, Bell O, Janser HG, Muckenthaler M, Schumann K, Hentze MW. 2005. Altered body iron distribution and microcytosis in mice deficient in iron regulatory protein 2 (IRP2). *Blood* 106:2580–2589. <http://dx.doi.org/10.1182/blood-2005-04-1365>.
 45. Zhu BM, McLaughlin SK, Na R, Liu J, Cui Y, Martin C, Kimura A, Robinson GW, Andrews NC, Hennighausen L. 2008. Hematopoietic-specific Stat5-null mice display microcytic hypochromic anemia associated with reduced transferrin receptor gene expression. *Blood* 112:2071–2080. <http://dx.doi.org/10.1182/blood-2007-12-127480>.
 46. Skaar EP. 2010. The battle for iron between bacterial pathogens and their vertebrate hosts. *PLoS Pathog* 6:e1000949. <http://dx.doi.org/10.1371/journal.ppat.1000949>.
 47. Pollack S, Fleming J. 1984. *Plasmodium falciparum* takes up iron from transferrin. *Br J Haematol* 58:289–293. <http://dx.doi.org/10.1111/j.1365-2141.1984.tb06087.x>.
 48. Sanchez-Lopez R, Haldar K. 1992. A transferrin-independent iron uptake activity in *Plasmodium falciparum*-infected and uninfected erythrocytes. *Mol Biochem Parasitol* 55:9–20. [http://dx.doi.org/10.1016/0166-6851\(92\)90122-Z](http://dx.doi.org/10.1016/0166-6851(92)90122-Z).
 49. Luzzi GA, Torii M, Aikawa M, Pasvol G. 1990. Unrestricted growth of *Plasmodium falciparum* in microcytic erythrocytes in iron deficiency and thalassaemia. *Br J Haematol* 74:519–524. <http://dx.doi.org/10.1111/j.1365-2141.1990.tb06344.x>.
 50. Mockenhaupt FP, Bienzle U, May J, Falusi AG, Ademowo OG, Olumese PE, Meyer CG. 1999. *Plasmodium falciparum* infection: influence on hemoglobin levels in alpha-thalassaemia and microcytosis. *J Infect Dis* 180:925–928. <http://dx.doi.org/10.1086/314959>.